

Magnetic properties and magnetocaloric effect in $RE_{55}Co_{30}Al_{10}Si_5$ (*RE*= Er and Tm) amorphous ribbons

Hao Sun(孙浩), Junfeng Wang(王俊峰), Lu Tian(田路), Jianjian Gong(巩建建), Zhaojun Mo(莫兆军), Jun Shen(沈俊), and Baogen Shen(沈保根)

Citation: Chin. Phys. B, 2022, 31 (**11**): 117503. DOI: 10.1088/1674-1056/ac8733

What follows is a list of articles you may be interested in

Large inverse and normal magnetocaloric effects in HoBi compound with nonhysteretic first-order phase transition

Yan Zhang(张艳), You-Guo Shi(石友国), Li-Chen Wang(王利晨), Xin-Qi Zheng(郑新奇), Jun Liu(刘俊), Ya-Xu Jin(金亚旭), Ke-Wei Zhang(张克维), Hong-Xia Liu(刘虹霞), Shuo-Tong Zong(宗朔通), Zhi-Gang Sun(孙志刚), Ji-Fan Hu(胡季帆), Tong-Yun Tong(赵同云), and Bao-Gen Shen(沈保根)

Chin. Phys. B, 2022, 31 (**7**): 077501. DOI: 10.1088/1674-1056/ac597f

Magnetic and magnetocaloric effect in a stuffed honeycomb polycrystalline antiferromagnet $GdInO_3$

Yao-Dong Wu(吴耀东), Wei-Wei Duan(段薇薇), Qiu-Yue Li(李秋月), Yong-Liang Qin(秦永亮),Zhen-Fa Zi(訾振发), and Jin Tang(汤进)

Chin. Phys. B, 2022, 31 (**6**): 067501. DOI: 10.1088/1674-1056/ac43a1

Magnetism and giant magnetocaloric effect in rare-earth-based compounds R_3BWO_9 (*R* = Gd, Dy, Ho)

Lu-Ling Li(李炉领), Xiao-Yu Yue(岳小宇), Wen-Jing Zhang(张文静), Hu Bao(鲍虎), Dan-Dan Wu(吴丹丹), Hui Liang(梁慧), Yi-Yan Wang(王义炎), Yan Sun(孙燕), Qiu-Ju Li(李秋菊), and Xue-Feng Sun(孙学峰)

Chin. Phys. B, 2021, 30 (**7**): 077501. DOI: 10.1088/1674-1056/abf916

Metamagnetic transition and reversible magnetocaloric effect in antiferromagnetic DyNiGa compound

Yan-Hong Ding(丁燕红), Fan-Zhen Meng(孟凡振), Li-Chen Wang(王利晨), Ruo-Shui Liu(刘若水), Jun Shen(沈俊)

Chin. Phys. B, 2020, 29 (**7**): 077501. DOI: 10.1088/1674-1056/ab90f3

Multicaloric and coupled-caloric effects

Jia-Zheng Hao(郝嘉政), Feng-Xia Hu(胡凤霞), Zi-Bing Yu(尉紫冰), Fei-Ran Shen(沈斐然), Hou-Bo Zhou(周厚博), Yi-Hong Gao(高怡红), Kai-Ming Qiao(乔凯明), Jia Li(李佳), Cheng Zhang(张丞), Wen-Hui Liang(梁文会), Jing Wang(王晶), Jun He(何峻), Ji-Rong Sun(孙继荣), Bao-Gen Shen(沈保根)

Chin. Phys. B, 2020, 29 (**4**): 047504. DOI: 10.1088/1674-1056/ab7da7

Magnetic properties and magnetocaloric effect in $RE_{55}Co_{30}Al_{10}Si_5$ (RE = Er and Tm) amorphous ribbons

Hao Sun(孙浩)[1,2], Junfeng Wang(王俊峰)[2], Lu Tian(田路)[2], Jianjian Gong(巩建建)[1,2], Zhaojun Mo(莫兆军)[2,†], Jun Shen(沈俊)[3], and Baogen Shen(沈保根)[1,‡]

[1] *School of Rare Earths, University of Science and Technology of China, Hefei* 230026, *China*
[2] *Ganjiang Innovation Academy, Chinese Academy of Sciences, Ganzhou* 341000, *China*
[3] *Key Laboratory of Cryogenics, Technical Institute of Physics and Chemistry, Chinese Academy of Sciences, Beijing* 100190, *China*

(Received 26 May 2022; revised manuscript received 6 July 2022; accepted manuscript online 5 August 2022)

The magnetic and magnetocaloric effects (MCE) of the amorphous $RE_{55}Co_{30}Al_{10}Si_5$ (RE = Er and Tm) ribbons were systematically investigated in this paper. Compounds with R = Er and Tm undergo a second-order magnetic phase transition from ferromagnetic (FM) to paramagnetic (PM) around Curie temperature $T_C \sim 9.3$ K and 3 K, respectively. For $Er_{55}Co_{30}Al_{10}Si_5$ compound, an obvious magnetic hysteresis and thermal hysteresis were observed at low field below 6 K, possibly due to spin-glass behavior. Under the field change of 0 T–5 T, the maximum values of magnetic entropy change ($-\Delta S_M^{max}$) reach as high as 15.6 J/kg·K and 15.7 J/kg·K for $Er_{55}Co_{30}Al_{10}Si_5$ and $Tm_{55}Co_{30}Al_{10}Si_5$ compounds, corresponding refrigerant capacity (RC) values are estimated as 303 J/kg and 189 J/kg, respectively. The large MCE makes amorphous $RE_{55}Co_{30}Al_{10}Si_5$ (RE = Er and Tm) alloys become very attractive magnetic refrigeration materials in the low-temperature region.

Keywords: magnetocaloric effect, amorphous, magnetic refrigeration, magnetic property

PACS: 75.30.Sg, 75.47.Np **DOI:** 10.1088/1674-1056/ac8733

1. Introduction

With the expanding demand for cryogenic refrigeration such as gas liquefaction and cryogenic superconductivity, the research on energy-efficient cryogenic refrigeration technology has become a hot theme.[1–3] Magnetic refrigeration based on the magnetocaloric effect has received significant attention due to its high energy efficiency and environmental friendliness.[4] Unfortunately, magnetic refrigeration is not yet widely used owing to the lack of suitable materials with large MCE.[5] Refrigerant capacity (RC) and the maximum values of magnetic entropy change ($-\Delta S_M^{max}$) are two critical parameters for evaluating the MCE of material, and improving their values has been the goal of efforts in the field of magnetic refrigeration.[6–12]

Amorphous alloys without boundaries and long-range order tend to exhibit attractive properties, such as corrosion resistance, adjustable phase transition temperatures, excellent RC, *etc.*, which has attracted extensive attention, especially in magnetic refrigeration region.[13–17] Among them, rare earth (RE)-based amorphous materials are expected to exhibit excellent MCE attributed to the large magnetic moments (μ_B) and total angular momentum quantum number (J) of RE ions. However, most of the RE-based amorphous materials usually show low $-\Delta S_M^{max}$ values despite their large RC, which restricts their application.[18] Therefore, it is of great interest to find amorphous alloys with large $-\Delta S_M^{max}$ and RC values in a suitable temperature range.

In recent years, numerous amorphous materials with large $-\Delta S_M^{max}$ values at low-temperature have been reported in the RE–Co–Al (RE = Gd–Tm) system. For example, the values of $-\Delta S_M^{max}$ reach 17.0 J/kg·K at 5.5 K for $Er_{32}Tm_{24}Co_{24}Al_{20}$,[19] 16 J/kg·K at 7 K for $Er_{48}Tm_8Co_{24}Al_{20}$,[19] 9.3 J/kg·K at 112 K for $Gd_{60}Co_{20}Al_{20}$,[20] 12.36 J/kg·K at 91 K for $Gd_{36}Tb_{20}Co_{20}Al_{24}$,[21] 10.1 J/kg·K at 112 K for $Gd_{55}Co_{25}Al_{20}$[22] under a field change ($\Delta\mu_0 H$) from 0 T–5 T, which are higher than that of most amorphous materials reported at the same temperature region.[17,18,22–27] $Gd_{55}Co_{30}Al_{15}$ microwire with potential application in the nitrogen liquefaction region was reported recently by Wang *et al.*,[28] whose $-\Delta S_M^{max}$ and RCP values can reach 9.71 J/kg·K and 572 J/kg under the $\Delta\mu_0 H$ of 0 T–5 T. It is well known that Tm-based and Er-based alloys typically have very low magnetic ordering transition temperature (T_{ord}) resulting from weak Ruderman–Kittel–Kasuya–Yosida (RKKY) interactions, which is highly valuable for potential applications in hydrogen liquefaction, space science and the fuel industry, *etc*. Therefore, $RE_{55}Co_{30}Al_{15}$ (RE = Tm and Er) amorphous alloys may be promising materials for magnetic refrigeration in the low-temperature region. To improve their glass-forming ability (GFA), 5-at.% Si element was introduced to substitute the equal content of Al.[29] In this paper, the quaternary $RE_{55}Co_{30}Al_{10}Si_5$ (RE = Tm and Er) amorphous alloys were

†Corresponding author. E-mail: mozhaojun@gia.cas.cn
‡Corresponding author. E-mail: shenbg@iphy.ac.cn

© 2022 Chinese Physical Society and IOP Publishing Ltd

successfully prepared, and their magnetic properties and MCE were systematically studied

2. Experimental details

Firstly, pre-alloyed ingots with a nominal composition of $RE_{55}Co_{30}Al_{10}Si_5$ (RE = Tm and Er) were fabricated by arcmelting the mixtures of pure metals in stoichiometric ratio under argon atmosphere. The purity of rare elements Er and Tm exceed 99.9%, and the purity of other ingredients is not less than 99.99%. Besides, an additional 5% RE components were added to compensate for evaporation losses. During the arcmelting process, the ingots were turned over and remelted four times to guarantee the homogeneity of the composition. Then, the molten pre-alloyed ingots heated by an induction coil were pressure sprayed with argon gas onto a single copper wheel with a linear surface velocity of 35 m/s. Finally, the structure and magnetic properties of the amorphous ribbons were measured. The structure of samples was ascertained by the x-ray diffraction (XRD) model Bruker D8A A25 in the range of the Bragg angles (2θ) from 25° to 85° using the Cu-$K\alpha$ radiation. The magnetic measurements were conducted using a commercial vibrating sample magnetometer (VSM), model PPMS-9 (Quantum Design).

3. Results and discussion

Room temperature XRD patterns of $RE_{55}Co_{30}Al_{10}Si_5$ (RE = Tm and Er) ribbons are illustrated in Fig. 1. Both compounds possess vast diffraction peaks and no sharp crystalline peaks, which is typical amorphous characteristics.

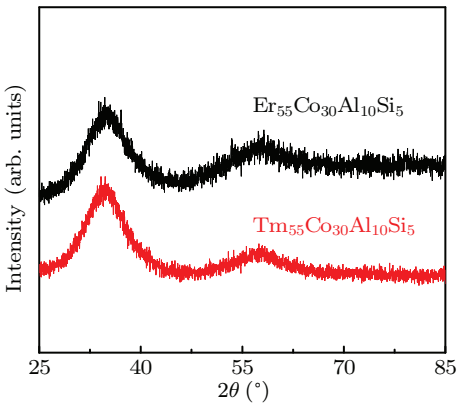


Fig. 1. Room temperature XRD patterns for $RE_{55}Co_{30}Al_{10}Si_5$ (RE = Tm and Er).

Figures 2(a) and 2(b) show the temperature T dependence of magnetization M (left-hand scale) measured by zero-field-cooled (ZFC) and field-cooled (FC) mode and the reciprocal susceptibility $1/\chi$ (right-hand scale) for $RE_{55}Co_{30}Al_{10}Si_5$ (RE = Er and Tm) under $\mu_0 H = 0.01$ T, respectively. It is observed there is a distinct discrepancy between the ZFC and FC branches of $Er_{55}Co_{30}Al_{10}Si_5$ at low temperature. The thermomagnetic irreversibility usually occurs in some amorphous materials with spin-glass systems.[13] In contrast, the ZFC and FC curves of $Tm_{55}Co_{30}Al_{10}Si_5$ are almost overlapping over the whole temperature ranges. The Curie–Weiss fit to the $1/\chi$–T curves of both compounds suggests that the values of $1/\chi$ at high temperature obey the Curie–Weiss law

$$\chi(T) = C/(T - \theta_P). \tag{1}$$

Here C is the Curie–Weiss constant, θ_P is the paramagnetic Curie temperature. Based on the result of Curie–Weiss fit, the values of θ_P deduced are 7.08 K and 0.17 K for $Er_{55}Co_{30}Al_{10}Si_5$ and $Tm_{55}Co_{30}Al_{10}Si_5$, respectively. The positive θ_P value indicates that the ferromagnetic (FM) interactions are dominant in these compounds. The Curie temperatures (T_C) of compounds with RE = Er and Tm are determined to be 9.3 K and 3 K, respectively, corresponding to the minimum of (dM_{FC}/dT)–T curves as shown in Figs. 2(c) and 2(d). Notably, the θ_P values for both compounds are significantly lower than their respective T_C values. The phenomenon is also observed in some Er-based and Tm-based ferromagnetic amorphous materials such as $Er_{60}Co_{20}Ni_{20}$,[26] $RE_{60}Co_{20}Al_{20}$ (RE = Er and Tm),[30] $RE_{55}Ni_{18}Al_{27}$ (RE = Er and Tm).[31] For these materials, their magnetic moments all derived from RE atoms, indicating that all magnetic interactions are related to RE atoms. Therefore, the characteristic may be associated with the crystalline electric field effects (CEF) due to the non-spherical symmetry of 4f electronic cloud for Er and Tm. Besides, it is clear seen from Fig. 2(c) that the thermomagnetic irreversibility between ZFC and FC occurs below 8 K and gradually increases with decreasing temperature.

The isothermal magnetization (M–$\mu_0 H$) curves in the vicinity of T_C for $RE_{55}Co_{30}Al_{10}Si_5$ (RE = Er and Tm) are given in Figs. 3(a) and 3(b). The magnetization of both alloys abruptly increases to tend saturation with the increasing field below T_C, reflecting a typical ferromagnetic feature. Figure 3(c) presents the M–$\mu_0 H$ curves in the mode of increasing and decreasing field from 0 T–0.5 T for $RE_{55}Co_{30}Al_{10}Si_5$ (RE = Er and Tm). Apparently, the $Er_{55}Co_{30}Al_{10}Si_5$ exhibits a large hysteresis at 2 K, which decreases with increasing temperature and almost disappears at 6 K. Nevertheless, no hysteresis is observed in $Tm_{55}Co_{30}Al_{10}Si_5$ at 2 K. Considering the thermomagnetic irreversibility of $Er_{55}Co_{30}Al_{10}Si_5$ also decreases with rising temperature and disappears completely at 8 K under $\mu_0 H = 0.01$ T. Therefore, it can be inferred that the hysteresis and thermomagnetic irreversibility may both originate from spin-glasses behavior. The M–$\mu_0 H$ curves of $Er_{55}Co_{30}Al_{10}Si_5$ in the mode of increasing field at various temperatures are demonstrated in Fig. 3(d). There are multiple crossover points for M–$\mu_0 H$ curves of $Er_{55}Co_{30}Al_{10}Si_5$ at various temperatures, which may lead to a positive magnetic entropy change at low temperature and low field.

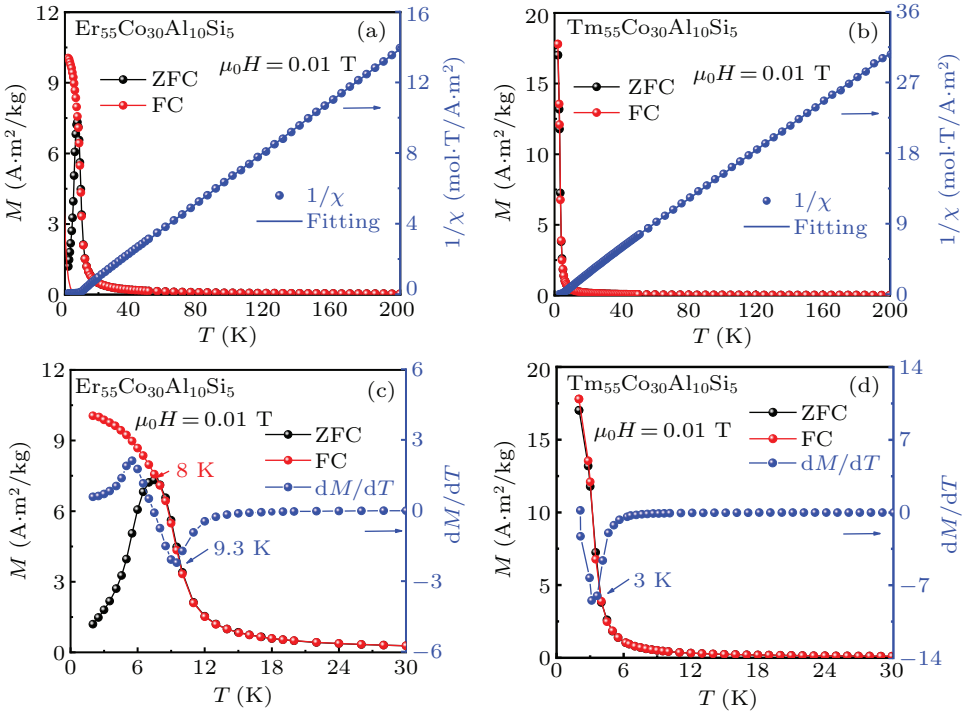


Fig. 2. The M–T curves (left-hand scale) in the mode of ZFC and FC and $(1/\chi)$–T curves (right-hand scale) of (a) $Er_{55}Co_{30}Al_{10}Si_5$ and (b) $Tm_{55}Co_{30}Al_{10}Si_5$ under $\mu_0 H = 0.01$ T. The M–T curves (left-hand scale) and (dM/dT)–T curves (right-hand scale) of (c) $Er_{55}Co_{30}Al_{10}Si_5$ and (d) $Tm_{55}Co_{30}Al_{10}Si_5$ in the temperature range from 0 K–30 K at $\mu_0 H = 0.01$ T.

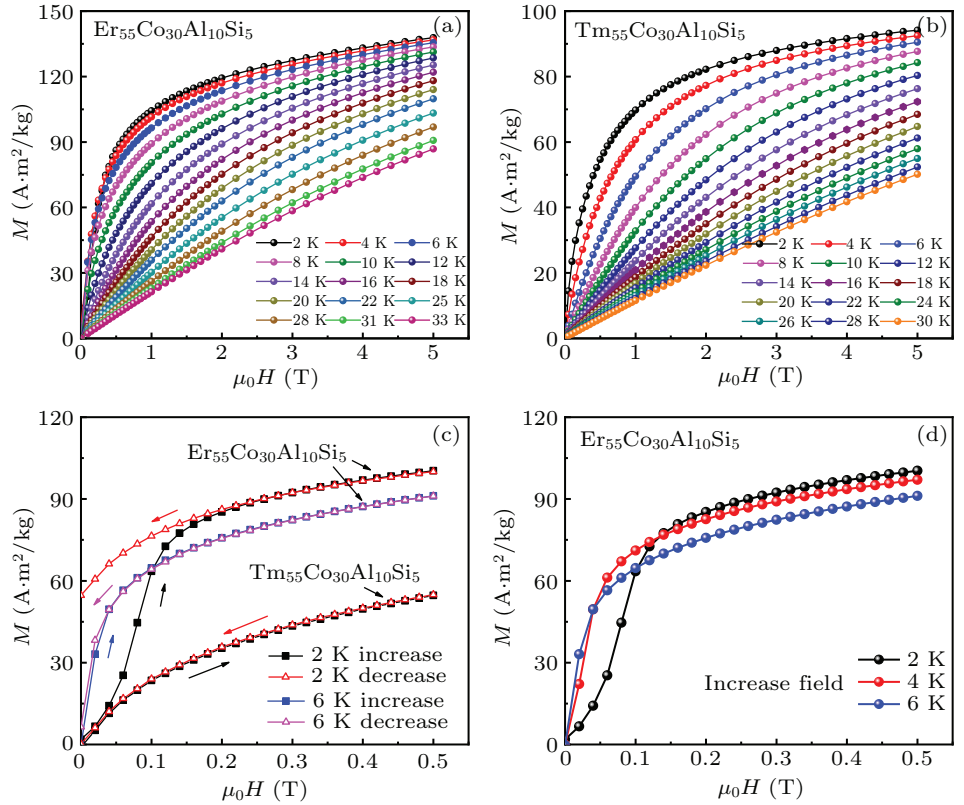


Fig. 3. The M–$\mu_0 H$ curves for (a) $Er_{55}Co_{30}Al_{10}Si_5$ and (b) $Tm_{55}Co_{30}Al_{10}Si_5$ at various temperatures under $\Delta\mu_0 H$ of 0 T–5 T. (c) The M–$\mu_0 H$ curves of $Er_{55}Co_{30}Al_{10}Si_5$ at 2 K and 6 K and $Tm_{55}Co_{30}Al_{10}Si_5$ at 2 K in the mode of increasing and decreasing magnetic fields from 0 T–0.5 T. (d) The M–$\mu_0 H$ curves of $Er_{55}Co_{30}Al_{10}Si_5$ at 2 K, 4 K, and 6 K measured by increasing field from 0 T–0.5 T.

The $-\Delta S_M^{max}$ is a highly important figure-of-merit to evaluate the MCE, calculated by the thermal-dynamic Maxwell relation given by

$$\Delta S_M(T,H) = \int_0^{H_{max}} \left(\frac{\partial M}{\partial T}\right)_H dH, \tag{2}$$

where H_{max} represents the maximum magnetic field that can be applied. The $-\Delta S_M$ versus T curves of $RE_{55}Co_{30}Al_{10}Si_5$ (RE = Er and Tm) under the $\Delta\mu_0 H$ from 0 T–1 T to 0 T–5 T are displayed in Fig. 4. The $-\Delta S_M^{max}$ values, at the $\Delta\mu_0 H = 0$ T–5 T, are determined to be 15.6 J/kg·K for $Er_{55}Co_{30}Al_{10}Si_5$ and 15.7 J/kg·K for $Tm_{55}Co_{30}Al_{10}Si_5$, respectively, which are higher than that of most reported RE-based amorphous materials.[13–26] The positive ΔS_M^{max} value of $Er_{55}Co_{30}Al_{10}Si_5$ at low temperature from 0 T–1 T may attribute to the spin glass behavior mentioned before. Moreover, it is worth noting that the $-\Delta S_M$ value of $Er_{55}Co_{30}Al_{10}Si_5$ is considerable over a wide temperature range above the spinglass freezing temperature, making it still attractive within temperatures free from hysteresis effect.

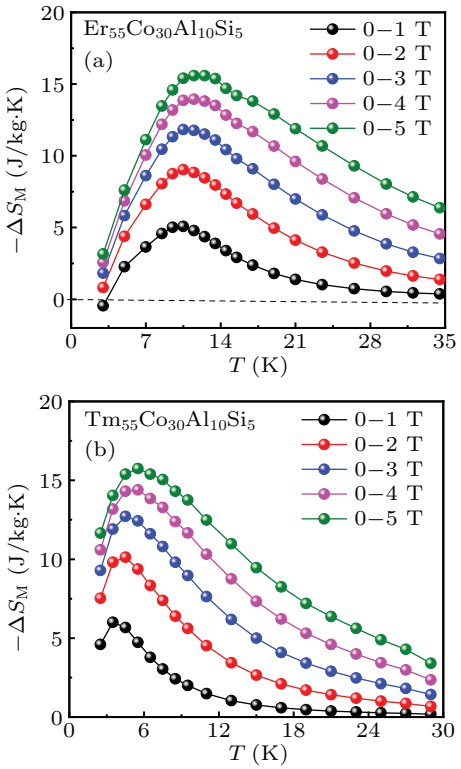


Fig. 4. The $-\Delta S_M$ versus T curves of $RE_{55}Co_{30}Al_{10}Si_5$ (RE = Er and Tm) under the $\Delta\mu_0 H$ for different magnetic field changes up to 5 T.

Moreover, a phenomenological universal curve was proposed to characterize the second-order nature of some ferromagnetic magnetocaloric materials, which is obtained by the reconstruction of the $-\Delta S_M$ versus T curves under the various $\Delta\mu_0 H$.[32] According to the definition of universal curve, the y coordinate of $-\Delta S_M$ versus T curve is rescaled to $\Delta S'$ calculated by

$$-\Delta S' = \Delta S_M(T)/\Delta S_M^{max}. \tag{3}$$

The x coordinate of $-\Delta S_M$ versus T curves is converted into θ, which is defined as follows:

$$\theta = \begin{cases} -(T-T_C)/(T_{r1}-T_C), & T \le T_C, \\ (T-T_C)/(T_{r2}-T_C), & T > T_C, \end{cases} \tag{4}$$

where T_{r1} and T_{r2} are temperatures of the two reference points corresponding to $0.6\times|\Delta S_M^{max}|$. The T_{r1} value is approximately estimated by extending the low end of $-\Delta S_M$ versus T curves to the point (0, 0), when low-temperature data are missing.

The rebuilding $\Delta S'$–θ curves of $RE_{55}Co_{30}Al_{10}Si_5$ (RE = Er and Tm) are shown in Fig. 5. It is striking that all curves for compounds with RE = Er and Tm under different $\Delta\mu_0 H$ are overlapped over the whole temperature range, which proves their second-order magnetic phase transition nature.

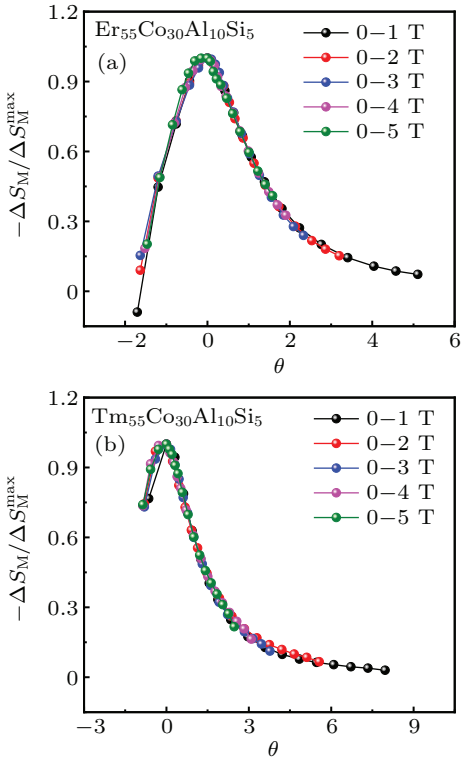


Fig. 5. Normalized magnetic entropy change as a function of the rescaled temperature for (a) $Er_{55}Co_{30}Al_{10}Si_5$ and (b) $Tm_{55}Co_{30}Al_{10}Si_5$ with $\Delta\mu_0 H$ from 0 T–1 T to 0 T–5 T.

Temperature-averaged magnetic entropy change (TEC) has been posted by Griffith *et al.* to judge the feasibility of material application in the magnetic refrigerator,[33] which can be expressed as

$$\mathrm{TEC}(\Delta T_{lift}) = \frac{1}{\Delta T_{lift}} \max_{T_{mid}} \left\{ \int_{T_{mid}-\Delta T_{lift}/2}^{T_{mid}+\Delta T_{lift}/2} \Delta S(T)_{(\Delta H,T)}\, \mathrm{d}T \right\}, \tag{5}$$

where the ΔT_{lift} represents temperature regime, T_{mid} represents the middle temperature point in which the TEC (ΔT_{lift}) value is the largest for a given ΔT_{lift}.

Besides, refrigerant capacity (RC) also has been widely applied to evaluate the cooling efficiency of the MCE materials, which reflects the amount of heat transfer from cold to hot tanks in an ideal refrigeration cycle. The value of RC is calculated by the following formula:

$$\mathrm{RC} = \int_{T_{cold}}^{T_{hot}} \Delta S_M(T)\, \mathrm{d}T, \tag{6}$$

where T_{hot} and T_{cold} represent the temperatures on either side corresponding to the half-peak value of $-\Delta S_M$ versus T

curves. For unidentifiable T_{cold} value beyond the measurement interval of the instrument, T_{cold} is considered to be 2.5 K, which is the lowest temperature the device can measure.

The calculated TEC(3) and RC as a function of $\Delta\mu_0 H$ for $RE_{55}Co_{30}Al_{10}Si_5$ (RE = Er and Tm) are plotted on Fig. 6 together with the $-\Delta S_M^{max}$ versus $\Delta\mu_0 H$ curves. The TEC(3) $\Delta\mu_0 H$ curves for both materials show a similar dependence on $\Delta\mu_0 H$, and their corresponding $-\Delta S_M^{max}$ and TEC(3) values are very close at any magnetic field, suggesting the existence of a stable platform at least $\Delta T_{lift} = 3$ K. The RC values of compounds with Er and Tm can reach $\sim$ 303 J/kg and $\sim$ 189 J/kg at the $\Delta\mu_0 H$ of 0 T–5 T, respectively, which also confirms the existence of a wide δT_{FWHM}.

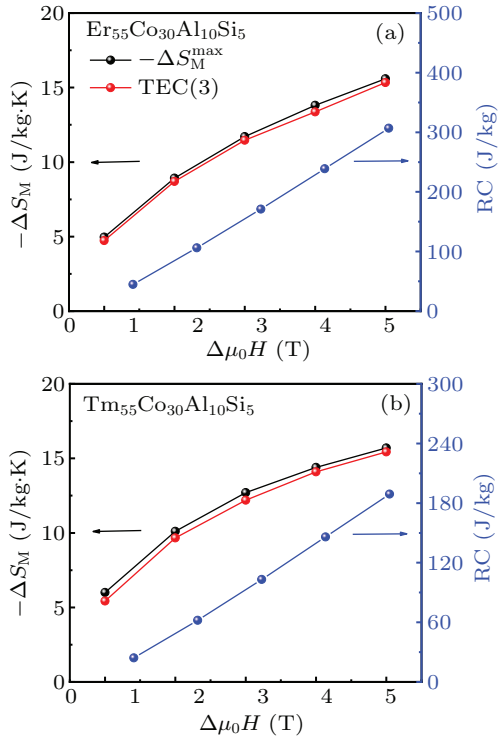


Fig. 6. TEC(3) and $-\Delta S_M^{max}$ (left axis), and RC (right axis) as a function of $\Delta\mu_0 H$ for $RE_{55}Co_{30}Al_{10}Si_5$ (RE = Er and Tm).

Table 1. The T_C, $|\Delta S_M^{max}|$, and RC parameters for $RE_{55}Co_{30}Al_{10}Si_5$ (RE = Er and Tm) and some reported promising MCE materials at low temperature under $\Delta\mu_0 H = 0$ T–5 T.

Materials	T_C	ΔS_M^{max} (J/kg·K)	RC (J/kg)	Refs.
$Tm_{55}Co_{30}Al_{10}Si_5$	3	15.6	189	present
$Er_{55}Co_{30}Al_{10}Si_5$	9.3	15.7	303	present
$Tm_{60}Al_{20}Ni_{20}$	4.4	14.1	$\sim$ 180	[34]
$Er_{60}Al_{20}Ni_{20}$	9.5	14.3	$\sim$ 280	[34]
$Tm_{60}Co_{20}Al_{20}$	5	15.06	243.4	[30]
$Er_{60}Co_{20}Al_{20}$	10.3	15.57	391.8	[30]
$Tm_{60}Ni_{30}Co_{10}$	6.3	14.2	$\sim$ 165	[35]
$Er_{60}Ni_{30}Co_{10}$	11.5	12.1	$\sim$ 230	[23]

To visually represent their excellent performance, several critical parameters (T_C, $-\Delta S_M^{max}$ and RC) of $RE_{55}Co_{30}Al_{10}Si_5$ (RE = Er and Tm) and some promising amorphous materials at low temperature were summarized in Table 1. Compared with other promising amorphous materials, the $-\Delta S_M^{max}$ and RC values of $RE_{55}Co_{30}Al_{10}Si_5$ (RE = Er and Tm) are comparable or even larger than those of them, which demonstrates both alloys are also very potential candidates in practical applications. In particular, the large $-\Delta S_M^{max}$ value of the $Tm_{55}Co_{30}Al_{10}Si_5$ amorphous in the liquid helium temperature region is very promising for its potential application.

4. Conclusion

Briefly, $RE_{55}Co_{30}Al_{10}Si_5$ (RE = Er and Tm) ribbons were prepared by conventional rapid quenching method, and their structural and magnetic properties were investigated. The XRD patterns confirmed the fully amorphous character of the $RE_{55}Co_{30}Al_{10}Si_5$ (RE = Er and Tm) ribbon. The $\Delta S'$–θ curves demonstrate that both alloys undergo a second-order magnetic transition of FM to PM near their respective T_C, which results in a considerable MCE. Besides, a significant hysteresis is observed in $Er_{55}Co_{30}Al_{10}Si_5$, which may result from spin-glass behavior. The values of $-\Delta S_M^{max}$ (RC) can reach 15.6 J/kg·K (303 J/kg) for $Er_{55}Co_{30}Al_{10}Si_5$ and 15.7 J/kg·K (189 J/kg) for $Tm_{55}Co_{30}Al_{10}Si_5$, which are comparable or even larger than other promising amorphous materials. Especially, the $Tm_{55}Co_{30}Al_{10}Si_5$ compound is a promising amorphous MCE material in the liquid helium temperature region.

Acknowledgements

Project supported by the National Natural Science Foundation of China (Grant Nos. 52171195 and 52171054), the National Natural Science Foundation for Distinguished Young Scholars (Grant No. 51925605), and the Scientific Instrument Developing Project of the Chinese Academy of Sciences (Grant No. YJKYYQ20200042).

References

[1] Geng H, Cui X Y, Weng J H, She H L and Wang W Q 2019 *Appl. Therm. Eng.* **157** 113640
[2] Ghorbani B, Mehrpooya M, Shirmohammadi R and Hamedi M H 2018 *J. Clean. Prod.* **179** 495
[3] Yildiz Y and Nalbant M 2008 *Int. J. Mach. Tool. Manu.* **48** 947
[4] Li L W and Yan M 2020 *J. Alloys Compd.* **823** 153810
[5] Gschneidner K A Jr, Pecharsky V K and Tsokol A O 2005 *Rep. Prog. Phys.* **68** 1479
[6] Zhang H and Shen B G 2015 *Chin. Phys. B* **24** 127504
[7] Gupta S and Suresh K G 2015 *J. Alloys Compd.* **618** 562
[8] Shen B G, Sun J R, Hu F X, Zhang H W and Cheng Z H 2009 *Adv. Mater.* **21** 4545
[9] Wu C, Ding D and Xia L 2016 *Chin. Phys. Lett.* **33** 016102
[10] Ma Y F, Tang B Z, Xia L and Ding D 2016 *Chin. Phys. Lett.* **33** 126101
[11] Ding D, Zhang Y Q and Xia L 2015 *Chin. Phys. Lett.* **32** 106101
[12] Ding D, Wang P, Guan Q, Tang M B and Xia L 2013 *Chin. Phys. Lett.* **30** 096104
[13] Luo L, Shen H X, Bao Y, Yin H, Jiang S D, Huang Y J, Guo S, Gao S Y, Xing D W, Li Z and Sun J F 2020 *J. Magn. Magn. Mater.* **507** 166856
[14] Hou L, Xiang X Y, Huang Y, Zhang B, Jiang C, Chen S S and Li W H 2021 *Appl. Phys. A* **127** 501
[15] Dong Z Q and Yin S H 2020 *J. Magn. Magn. Mater.* **495** 165888

[16] Li J, Xue L, Yang W M, Yuan C C, Huo J T and Shen B L 2018 *Intermetallics* **96** 90
[17] Wang Z W, Yu P, Cui Y T and Xia L 2016 *J. Alloys Compd.* **658** 598
[18] Boutahar A, Lassri H, Zehani K, Bessais L and Hlil E K 2014 *Magn. Magn. Mater.* **369** 92
[19] Kou X H, Luo Q, Dinh P N and Shen J 2016 *J. Alloys Compd.* **699** 591
[20] Fu H and Zou M 2011 *J. Alloys Compd.* **509** 4613
[21] Yin H, Huang Y J, Bao Y, Jiang S, Xue P, Jiang S S, Wang H, Qin F X, Li Z, Sun S C, Wang Y F, Shen H X and Sun J F 2020 *J. Alloys Compd.* **815** 150983
[22] Yu P, Zhang N Z, Cui Y T, Wen L, Zeng Z Y and Xia L 2016 *J. Alloys Compd.* **655** 353
[23] Gao W L, Wang X J, Wang L J, Zhang Y K and Cui J Z 2018 *J. Non-Cryst. Solids* **484** 36
[24] Tang B Z, Huang L W, Song M N, Ding D, Wang X and Xia L 2019 *J. Non-Cryst. Solids* **522** 119589
[25] Li Z, Ding D and Xia L 2017 *Intermetallics* **86** 11
[26] Wang Y M, Guo D, Wu B B, Geng S H and Zhang Y K 2020 *J. Magn. Magn. Mater.* **498** 166179
[27] Zheng Z G, Zhong X C, Su K P, Yu H Y, Liu Z W, Zeng D C 2011 *Sci. China- Ser. G* **54** 1267
[28] Wang Y F, Duc N T M, Feng T F, Wei H J, Qin F X and Phan M H 2022 *J. Alloys Compd.* **907** 164328
[29] Lindner N, Sniadecki Z, Kolodziej M, Greneche J M, Marcin J, Skorvanek I and Idzikowski B 2022 *J. Mater. Sci.* **57** 553
[30] Zhang Y K, Zhun J, Li S, Zhang B, Wang Y M, Wang J and Ren Z M 2022 *J. Alloys Compd.* **895** 162633
[31] Jia Y S, Zhao X Y, Liu X L and Li L W 2020 *J. Alloys Compd.* **813** 152177
[32] Franco V and Conde A 2010 *Int. J. Refrig.* **33** 465
[33] Griffith L D, Mudryk Y, Salaughter J and Pecharsky V K 2018 *J. Appl. Phys.* **123** 034902
[34] Zhang Y K, Gao D, Wu B B, Wang H F, Guan R G, Li X and Ren Z M 2020 *J. Appl. Phys.* **127** 033905
[35] Guo D, Zhang Y K, Geng S H, Xu H, Ren Z M and Wilde G 2018 *J. Mater Sci.* **53** 9816